Electric scale-up for a slag heating furnace

Alfredo Bermúdez[*], Vincent Cregan[†], Dolores Gómez[‡], Ángel Rial[§], Rafael Vázquez[¶], Svenn Anton Halvorsen[‖]

Abstract

The aim of this study group is to contribute to the mathematical modelling and numerical simulation of a slag heating furnace. Two parallel studies were performed; one on numerical simulation of the process using a Finite Element Method software, while the other focused on non-dimensional thermal analysis of an electrode. Both studies provided preliminary results which are important stepping stones for a broad understanding of process relevant issues related to scale-up.

Keywords | electric slag heating; eddy-currents; nondimensional heat model

AMS classification |35Q61, 65N30

1. Introduction

Teknova AS is a research institute for science and technology established in 2007 in the southern part of Norway. Among its primary objectives is to create a bond between the University of Agder, Agder Research, and the industry and commerce in the region and outside.

Recently, Teknova, in cooperation with several business and research partners, started a project funded with 3 million NOK (around 375 000 EUR) by the Regional Research Fund Agder. The project focuses on efficient development of metallurgical processes from laboratory to pilot scale through

[*]Universidade de Santiago de Compostela and ITMATI; alfredo.bermudez@usc.es
[†]Centre de Recerca Matemática. Universitat Autónoma de Barcelona; vcregan@crm.cat
[‡]Universidade de Santiago de Compostela and ITMATI; mdolores.gomez@usc.es
[§]Universidade de Santiago de Compostela; angel.rial@usc.es
[¶]Istituto di Matematica Applicata e Tecnologie Informatiche; vazquez@imati.cnr.it
[‖]Teknova AS; sah@teknova.no

mathematical modelling tools and methods that safeguard the critical process capabilities during scale-up. The research is performed in close cooperation with researchers in production companies, and is based on cases provided by the industry itself.

The industrial project partners have excellent facilities for piloting of metallurgy and other processing. The companies are members of the Eyde-network that was established as an important cluster organization and motor for industrial development in South-Norway in 2007. Currently, the cluster companies are establishing the Eyde Innovation Centre which will constitute the core of their common research activities. Teknova cooperates closely with the Eyde cluster and intends, among others, to supply relevant mathematical models, simulations tools and know-how for proper scale-up.

The problem presented to the ESGI 97 lies in this context and it is related to the electric scale-up for a slag heating furnace. A more detailed description is given in the next section.

2. Challenge description

Consider a possible slag process where the slag is more heavy than the metal. Consider a cylindrical reactor with side electrodes. For an experimental lab/pilot furnace a four electrode system with power control of two electric circuits is considered, compared to a three-phase alternative. For an industrial or large pilot, only a three-phase system seems appropriate. A schematic side-view of a reactor electrode is given in Fig. 1.

The focus of the study group was on the electrical part of a possible reactor and how to do a proper electrical scale-up. More precisely,

- Possible issues/problems going from a four-electrode system to three-phase electrodes.
- How to scale up the power for a three-phase reactor from typical lab scale, via pilot, to small industrial scale.

The group split into two teams examining different aspects of the problem. On one hand, the mathematical modelling and numerical simulation of the electromagnetic process. On the other, the statement of a nondimensional model dealing with the thermal phenomena.

3. Study of the electromagnetic problem

3.1. The time-harmonic eddy currents model

To calculate the electromagnetic field we must solve Maxwell's equations. Since the electrodes are supplied with a sinusoidal current and the medium is as-

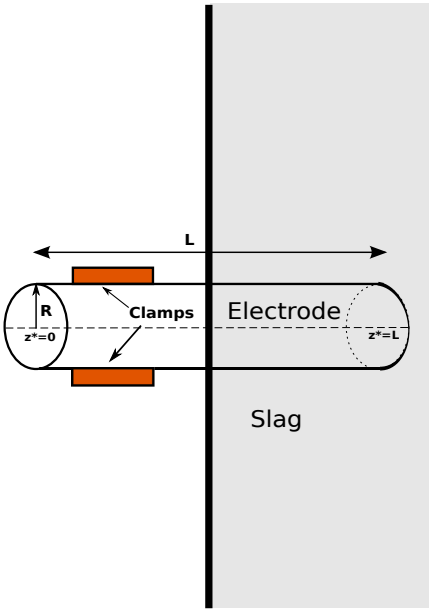

Figure 1: Close-up of one of the reactor electrodes.

sumed to be magnetically linear, the time harmonic approach is used. Thus, we can consider that all fields vary harmonically with time on the form

$$\mathcal{F}(\mathbf{x}, t) = \mathrm{Re}\,[\mathrm{e}^{i\omega t}\,\mathbf{F}(\mathbf{x})], \tag{1}$$

where t is time, $\mathbf{x} \in \mathbb{R}^3$ is the spatial variable, i is the imaginary unit, $\mathbf{F}(\mathbf{x})$ is the complex amplitude of field $\mathcal{F}$ and ω is the angular frequency, $\omega = 2\pi f$, f being the frequency of the alternating current.

Moreover, in the low-frequency harmonic regime, the term in Ampere's law including the electric displacement can be neglected (see, for instance, reference [4]).

Under these assumptions, the Maxwell's equations reduce to the so-called *eddy current* model

$$\mathbf{curl}\,\mathbf{H} = \mathbf{J}, \tag{2}$$

$$i\omega\mathbf{B} + \mathbf{curl}\,\mathbf{E} = \mathbf{0}, \tag{3}$$

$$\mathrm{div}\,\mathbf{B} = 0, \tag{4}$$

to which we have to add the data of the intensity current, I, flowing in the electrodes. Equations (2)-(4) hold on the whole space $\mathbb{R}^3$. The vectorial fields $\mathbf{H}$, $\mathbf{J}$, $\mathbf{B}$ and $\mathbf{E}$ are the complex amplitudes associated with the magnetic field, the current density, the magnetic induction and the electric field, respectively.

The system above needs to be completed by the constitutive relation

$$\mathbf{B} = \mu\mathbf{H}, \tag{5}$$

which take into account material properties through their magnetic permeability μ. We also need Ohm's law

$$\mathbf{J} = \sigma \mathbf{E}, \tag{6}$$

where σ denotes the electric conductivity, which is assumed to be a positive constant in conductors and null in dielectrics.

We notice that, since $\omega \neq 0$, equation (4) follows from equation (3). As we will see later, equations (2) and (3) can be solved using a suitable formulation leading to $\mathbf{H}$ in the whole domain and $\mathbf{J}$ in conductors. Then, $\mathbf{E}$ can be uniquely determined in conductors by $\mathbf{E} = \mathbf{J}/\sigma$. In this case, solving for $\mathbf{E}$ in the dielectrics is not required since it is not relevant for this problem.

To solve the equations above, we restrict them to a simply connected 3D bounded domain Ω consisting of two disjoint parts, Ω_{C} and Ω_{D}, occupied by conductors (the slag and electrodes) and dielectric (air), respectively (see Fig. 2). The domain Ω is assumed to have a Lipschitz-continuous connected boundary Γ. We denote by $\Gamma_{\mathbf{C}}$ and Γ_{D} the open surfaces such that $\bar{\Gamma}_{\mathrm{C}} := \partial\Omega_{\mathrm{C}} \cap \Gamma$ is the outer boundary of the conducting domain and $\bar{\Gamma}_{\mathrm{D}} := \partial\Omega_{\mathrm{D}} \cap \Gamma$ that of the dielectric domain. We also denote by $\mathbf{n}$ a unit normal vector to a given surface.

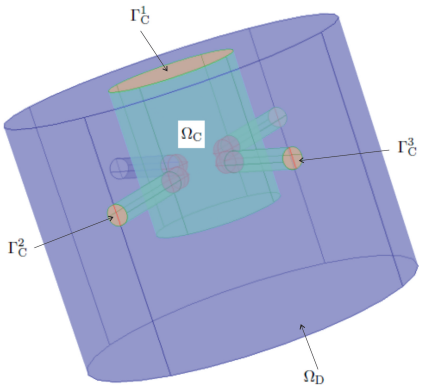

Figure 2: Sketch of the domain and nomenclature used in the mathematical model.

We assume that the outer boundary of the conductor $\partial\Omega_{\mathrm{C}} \cap \Gamma$ has L disjoint connected components $\Gamma_{\mathbf{C}}^n$, being the closure of open surfaces of two types: surfaces where the current intensity is prescribed (for instance $\Gamma_{\mathbf{C}}^2$ or $\Gamma_{\mathbf{C}}^3$ in Fig. 2), or surfaces where the potential is given (boundary $\Gamma_{\mathbf{C}}^1$ in Fig. 2). We denote $\Gamma_{\mathbf{C}} := \Gamma_{\mathbf{C}}^1 \cup \cdots \cup \Gamma_{\mathbf{C}}^L$. Notice that for this particular problem $L = 4$ or 5 depending on whether we consider 3 or 4 electrodes.

We have to complete the model with suitable boundary conditions. Let us consider the following ones:

$$\mathbf{E} \times \mathbf{n} = \mathbf{0} \quad \text{on } \Gamma_{\mathbf{C}}, \tag{7}$$

$$\mu \mathbf{H} \cdot \mathbf{n} = 0 \quad \text{on } \Gamma. \tag{8}$$

Condition (7) means that the electric current enters domain Ω perpendicular to the boundary whereas condition (8) implies that the magnetic field is tangential to the boundary.

Let us suppose that the boundary data consist of the voltage drops V_n, for $n = 1, \ldots, \widehat{L}$, and the input current intensities through each surface $\Gamma_{\mathbf{C}}^n$, I_n, for $n = \widehat{L}+1, \ldots, L$. We notice that the latter can be written as

$$\int_{\Gamma_{\mathbf{C}}^n} \mathbf{J} \cdot \mathbf{n} \, \mathrm{d}A = \mathrm{I}_n, \quad n = \widehat{L}+1, \ldots, L.$$

We summarize the strong problem defined in Ω to be solved:

$$i\omega \mathbf{B} + \mathbf{curl}\, \mathbf{E} = \mathbf{0}, \tag{9}$$

$$\mathbf{curl}\, \mathbf{H} = \mathbf{J}, \tag{10}$$

$$\operatorname{div} \mathbf{B} = 0, \tag{11}$$

$$\mathbf{B} = \mu \mathbf{H}, \tag{12}$$

$$\mathbf{J} = \sigma \mathbf{E}, \tag{13}$$

$$\mathbf{E} \times \mathbf{n} = \mathbf{0} \quad \text{on } \Gamma_{\mathbf{C}}, \tag{14}$$

$$\mu \mathbf{H} \cdot \mathbf{n} = 0 \quad \text{on } \Gamma, \tag{15}$$

$$\mathrm{V} = \mathrm{V}_{\mathrm{C}}^n \quad \text{on } \Gamma_{\mathbf{C}}^n, \ n = 1, \ldots, \widehat{L}, \tag{16}$$

$$\int_{\Gamma_{\mathbf{C}}^n} \mathbf{J} \cdot \mathbf{n} \, \mathrm{d}A = \mathrm{I}_n, \quad n = \widehat{L}+1, \ldots, L. \tag{17}$$

3.2. Magnetic vector potential/scalar electric potential formulation

Many formulations and finite element techniques to solve eddy current problmes in three dimensional bounded domains can be found in the literature (see [1, 3]. Here, we have chosen that based on the scalar and the magnetic vector potential.

Firstly, from (11), (15) and [6, Theorem 1.3.6] we deduce the existence of a vector field $\mathbf{A} \in \mathbf{H}(\mathbf{curl}, \Omega)$ called magnetic vector potential such that

$$\mathbf{curl}\, \mathbf{A} = \mathbf{B} \text{ in } \Omega, \tag{18}$$

$$\operatorname{div} \mathbf{A} = 0 \text{ in } \Omega, \tag{19}$$

$$\mathbf{A} \times \mathbf{n} = \mathbf{0} \text{ on } \Gamma. \tag{20}$$

The latter equality guarantees boundary condition (15) (see [2])

By replacing (18) in (9) we obtain

$$\mathbf{curl}(i\omega\mathbf{A}+\mathbf{E})=\mathbf{0} \text{ in } \Omega,$$

and then, in particular, there exists a scalar potential V such that

$$i\omega\mathbf{A}+\mathbf{E}=-\operatorname{grad}\mathrm{V} \text{ in } \Omega. \tag{21}$$

Therefore, the magnetic and electric fields can be written in terms of these potentials as follows:

$$\mathbf{E}=-i\omega\mathbf{A}-\operatorname{grad}\mathrm{V},$$
$$\mathbf{H}=\frac{1}{\mu}\,\mathbf{curl}\,\mathbf{A}.$$

From (14) and (20) we deduce

$$\operatorname{grad}_\Gamma \mathrm{V}:=\mathbf{n}\times\operatorname{grad}\mathrm{V}\times\mathbf{n}=-\mathbf{n}\times\mathbf{E}\times\mathbf{n}=\mathbf{0} \quad \text{on } \Gamma_{\mathbf{C}},$$

which implies that V must be constant on each connected component of $\Gamma_{\mathbf{C}}$.

From (9), (12), (13) and (21) we deduce

$$\sigma(i\omega\mathbf{A}+\operatorname{grad}\mathrm{V})+\mathbf{curl}(\frac{1}{\mu}\,\mathbf{curl}\,\mathbf{A})=\mathbf{0} \text{ in } \Omega. \tag{22}$$

We notice that, since $\sigma=0$ in Ω_{D}, we only need to compute V in Ω_{C}.

Finally, from (13) and (21), boundary conditions (17) become

$$\int_{\Gamma_{\mathbf{C}}^n}\sigma(i\omega\mathbf{A}+\operatorname{grad}\mathrm{V})\cdot\mathbf{n}\,\mathrm{dS}=-\mathrm{I}_n, \quad n=\widehat{L}+1,\ldots,L. \tag{23}$$

Summarizing, the problem to be solved reads as follows:

Given complex numbers $\mathrm{V}_{\mathrm{C}}^n$, $n=1,\ldots,\widehat{L}$ *and* I_n, $n=\widehat{L}+1,\ldots,L$, *find a vector field* $\mathbf{A}$ *defined in* Ω, *and a scalar field* V *defined in* Ω_{C} *and null on* $\Gamma_{\mathbf{C}}^n$, $n=\widehat{L}+1,\ldots,L$, *such that*

$$\sigma(i\omega\mathbf{A}+\operatorname{grad}\mathrm{V})+\mathbf{curl}(\frac{1}{\mu}\,\mathbf{curl}\,\mathbf{A})=\mathbf{0} \text{ in } \Omega, \tag{24}$$
$$\operatorname{div}\mathbf{A}=0 \text{ in } \Omega, \tag{25}$$
$$\mathbf{A}\times\mathbf{n}=0 \text{ on } \Gamma, \tag{26}$$
$$\sigma(i\omega\mathbf{A}+\operatorname{grad}\mathrm{V})\cdot\mathbf{n}=0 \text{ on } \partial\Omega_{\mathrm{C}}\setminus\Gamma_{\mathbf{C}}, \tag{27}$$
$$\mathrm{V}=\mathrm{V}_{\mathrm{C}}^n \text{ on } \Gamma_{\mathbf{C}}^n,\ n=1,\ldots,\widehat{L}, \tag{28}$$
$$\int_{\Gamma_{\mathbf{C}}^n}\sigma(i\omega\mathbf{A}+\operatorname{grad}\mathrm{V})\cdot\mathbf{n}\,\mathrm{dS}=-\mathrm{I}_n,\ n=\widehat{L}+1,\ldots,L. \tag{29}$$

For more details about this formulation, we refer the reader to [2].

3.3. Numerical simulation

In this section we present some results obtained from the numerical simulation of the problem. All FEM models, meshes and calculations were performed with the Comsol Multiphysics® 4.3 software, and in particular with the AC/DC module.

3.3.1 Geometry definition

A simple sketch of the reactor is composed by a pot, which contains the slag and a metal layer above the slag, and graphite electrodes. In order to deal with a more simple geometry, neither the pot nor the metal above the pot have been included. Instead, suitable boundary conditions have been considered. Thus, the domain reduces to the slag and to the electrodes carrying the electric current. We will consider the case of systems consisting of four or three electrodes. In order to perform suitable FEM numerical computations, this domain has been enclosed in a cylindrical artificial domain containing air around the device as illustrated in Fig. 3.

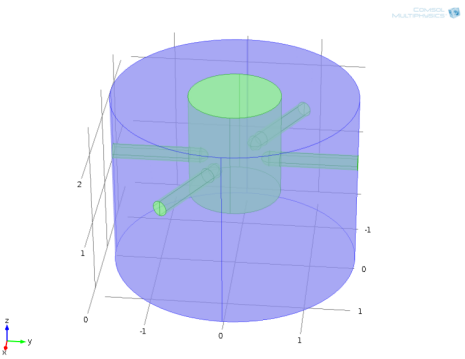

Figure 3: Computational domain for the four electrode configuration.

Moreover, the geometry has been constructed according to certain parameters that allow greater flexibility in the study. These parameters have been included in Fig. 4 and summarized in Table 1. In the four electrode system the angle θ between the electrodes has been set equal to 60°, while for the alternative three electrode configuration they are disposed conforming an equilateral triangle.

The domain has been discretized into tetrahedral elements (see Fig. 5). As it is well-known, the quality of the mesh is crucial to obtain an accurate solution with a reduced number of elements and so a reasonable computational time. Thus, in electrode contact areas, where the current density is higher, the mesh density is refined (see Fig. 5). In the four-electrode case, the complete mesh consists of 174812 elements and 1354563 degrees of freedom, while for the

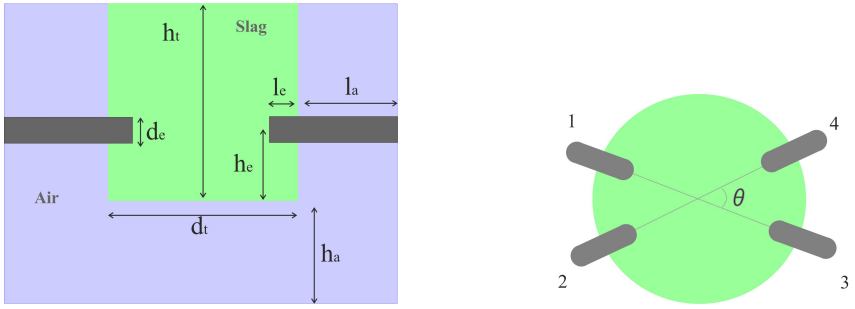

Figure 4: Sketch of a possible lab reactor. Parameters considered when constructing the geometry are detailed. Electrode pairs 1-3 and 2-4 are connected to different transformers.

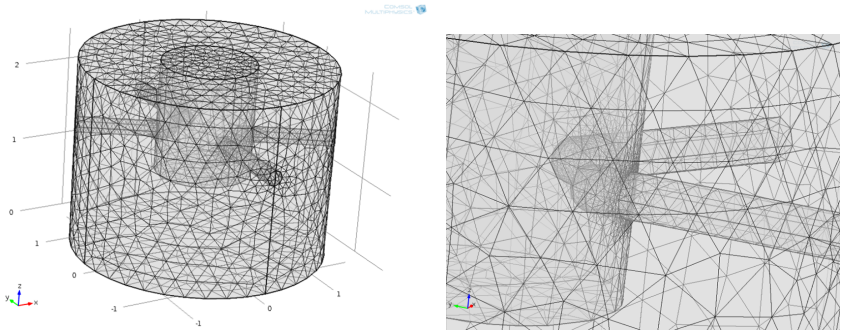

Figure 5: Mesh of the domain and detail in the electrodes contact areas.

three electrode configuration 132001 elements and 338087 degrees of freedom are considered. These meshes could probably be improved, but due to time constraints the working group did not consider this task. Even so, in the three-electrode case, we have compared the volumetric resistive losses obtained from different meshes to verify that the results are relatively accurate.

When working with alternating current, the electric current tends to become distributed within a conductor in such a way that the current density is higher near the surface of the conductor. This fact is called skin effect. The skin depth, δ is defined as the depth below the surface of the conductor at which the current density has fallen to 1/e from its value at the surface and in normal cases it is well approximated by the formula

$$\delta \simeq \sqrt{\frac{1}{\pi \mu \sigma f}}. \tag{30}$$

If the skin effect takes place, the skin depth is an important parameter to take into account when building the mesh if one wants to reproduce the field near the surface in an appropriate way. This is not the case in the actual

Parameter	Description	Value (mm)
d_t	Tank diameter	1200
h_t	Tank height	1400
h_e	Electrode height from tank bottom	500
d_e	Electrode diameter	200
l_e	Electrode length in tank	150
l_a	Electrode length in air	1000
h_a	Air height below tank	1000

Table 1: Geometrical data for the simulations.

Parameter	Value
Frequency	50 Hz
Intensity	14000 A

Table 2: Operation conditions.

computations, since skin effect is not relevant. Indeed, for a 50 Hz working frequency, the skin-depth in the graphite is around 258 mm and the diameter of the electrode is 200 mm. The same occurs in the slag: the skin-depth is about 4768 mm and the dimensions considered in the simulation are smaller than this quantity (see Tables 1 and 3).

3.3.2 Operational conditions and physical parameters

The operational conditions chosen for the simulations are summarized in Table 2. These data and the data considering the geometry considered in the previous section, are reasonable for a potential pilot but do not correspond to actual plans. In the modelling example, the RMS value of the electrode currents is $I = 14000$ A. In the four data electrode configuration, every electrode pair has its own independent supply source (electrode pairs 1-3 and 2-4 are connected to different transformers). It means that the current trajectory in the slag can close only in the limitations of one source, so the currents flow from lower electrodes to opposite upper electrodes. In the three-electrode system, the electrode currents are the same with 120° phase delay among them (three-phase current).

The input data given to Comsol Multiphysics® is the current density at the entry of each electrode which is computed as the quotient of the intensity and the input surface area. Thus, the current density is fixed and assumed to be homogeneously distributed on the input surface. Actually, induced currents contribute significantly to a non-uniform current distribution on this surface;

Material	Rel. permeability	Conductivity (S/m)	Skin depth (mm)
Graphite	1	$24 \cdot 10^4$	258
Slag	1	700	4768
Air	1	0.00001	

Table 3: Values of physical properties of materials and skin depth at 50 Hz.

this fact has not been considered in the present model due to software package constraints. Anyway, the error in current distribution only affects the part of the electrode close to its entry surface

Table 3 lists the values assigned to the physical properties for the different materials and the skin depth in conductors at a frequency of 50 Hz.

We note that the electrical conductivity assigned to air is not zero, but rather very small. Again this was motivated by some restrictions derived from the model used by the numerical simulation in Comsol Multiphysics®. To the study group's best knowledge, the A-V formulation implemented in this software does not allow to solve for two different domains (conductor and air) simultaneously. This is the motivation for solving the problem as if the whole domain were a conducting domain, but assigning a small conductivity to the air. In fact setting $\sigma = 0$ in the air leads to a singular matrix, and therefore the algebraic system resulting from the FEM formulation cannot be solved.

3.3.3 Boundary conditions setting

One of the main difficulties in studying the eddy current problem in a bounded domain is defining appropriate boundary conditions. These conditions must be mathematically suitable for the problem to be well posed, but at the same time physically realistic in the sense of involving only data actually attainable in practical scenarios.

The boundary conditions have been summarized in Fig. 6. In all the exterior boundaries of the domain the `Magnetic Insulation` ($\mathbf{A} \times \mathbf{n} = \mathbf{0}$) boundary condition is imposed (default condition in Comsol Multiphysics®). This condition forces the field $\mathbf{B}$ to be tangential to the exterior boundaries, which with the cylindrical shape of the outer domain is a reasonable approximation to reality. Comsol Multiphysics® automatically applies this boundary condition through the exterior boundary of the domain. A supplementary boundary condition is needed in order to obtain a unique potential V. By default, Comsol Multiphysics® uses the `Electric Insulation` ($\mathbf{J} \cdot \mathbf{n} = \mathbf{0}$) boundary condition, which we impose on the boundary corresponding to the air. On the input surface of each electrode the current density is given by imposing a `Normal current density` boundary condition ($-\mathbf{n} \cdot \mathbf{J} = J_i$). In fact, following the model stated in Section 3.2, the data would be the intensity instead of

the current density. As we have mentioned before, this would allow to compute the true current distribution in the electrodes instead of assuming that it is uniformly distributed on the entry surface. Finally, on the top part of the reactor the potential is given via the `Electric potential` option and we choose V=0. The reason is that, on one hand, the potential is constant on this boundary and, on the other, the potential is defined up to a constant on each connected component of the conducting domain (see Section 3.2). Then, on one boundary of each connected component we can set V=0.

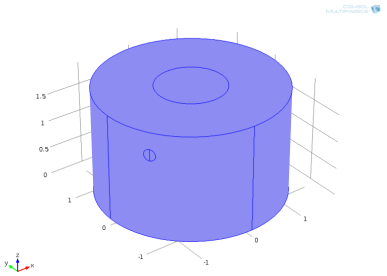

Magnetic insulation $\mathbf{A} \times \mathbf{n} = \mathbf{0}$

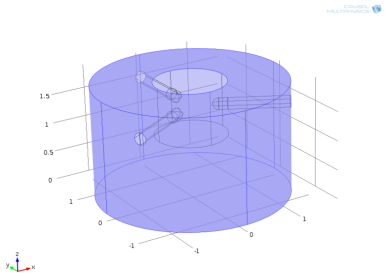

Electric insulation $\mathbf{J} \cdot \mathbf{n} = \mathbf{0}$

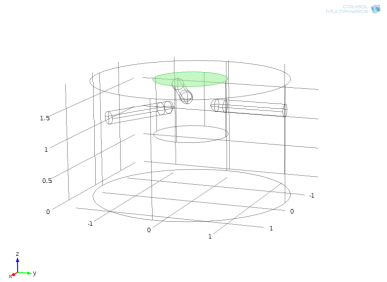

Electric potential V=0

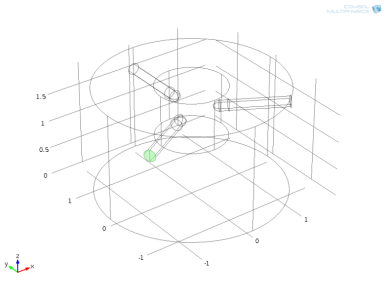

Normal current density $-\mathbf{n} \cdot \mathbf{J} = J_i$

Figure 6: Boundary conditions.

3.3.4 Numerical results for the four-electrode configuration

As mentioned in the previous section, for this case we have two separate electrode pairs supplied with 50 Hz AC single phase power.

In Figures 7 and 9 we show the Joule effect (or resistive losses) in the slag and electrodes, respectively, by using a slice plot. Figure 8 also shows the Joule effect in the slag but for demonstration purposes the maximum values of the field have been removed. In Figures 10, 11 and 12 a horizontal view has been employed to illustrate the Joule effect in the electrodes and slag. Figures 13 and 14 show the current density in the slag from different plane views.

From these pictures we deduce that the resulting current distribution within

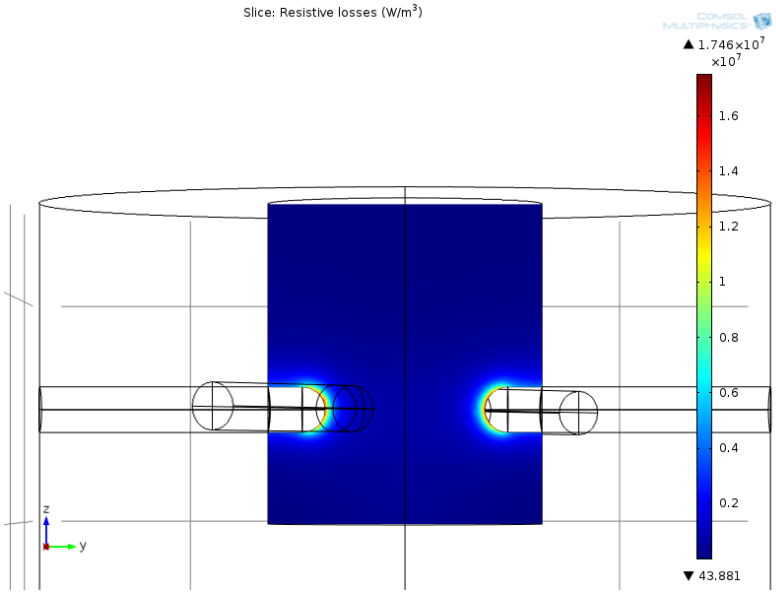

Figure 7: Joule effect (W/m^3) in the slag. yz view.

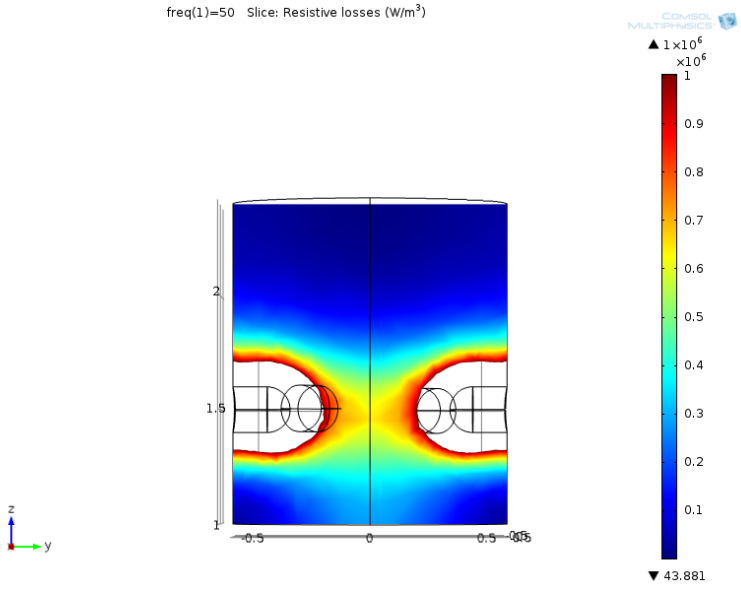

Figure 8: Joule effect (W/m^3) in the slag. Scale range. yz view.

the slag is affected by the mutual influence of neighbouring electrodes of the magnetic fields, the so-called "proximity effect". This effect is more obvious in the parts of the electrodes closer to the neighbouring electrodes. This is not the case in the three-electrode configuration (see Fig. 19) where the resistive

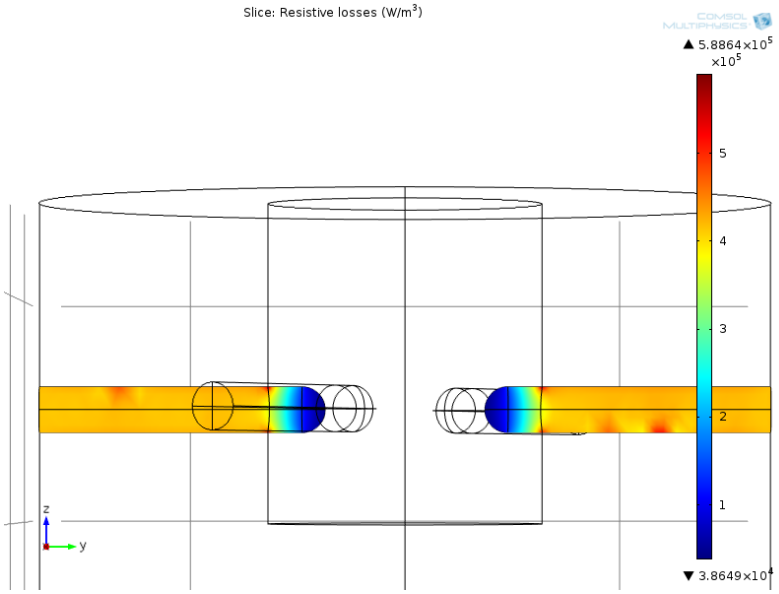

Figure 9: Joule effect (W/m^3) in the electrodes. yz view.

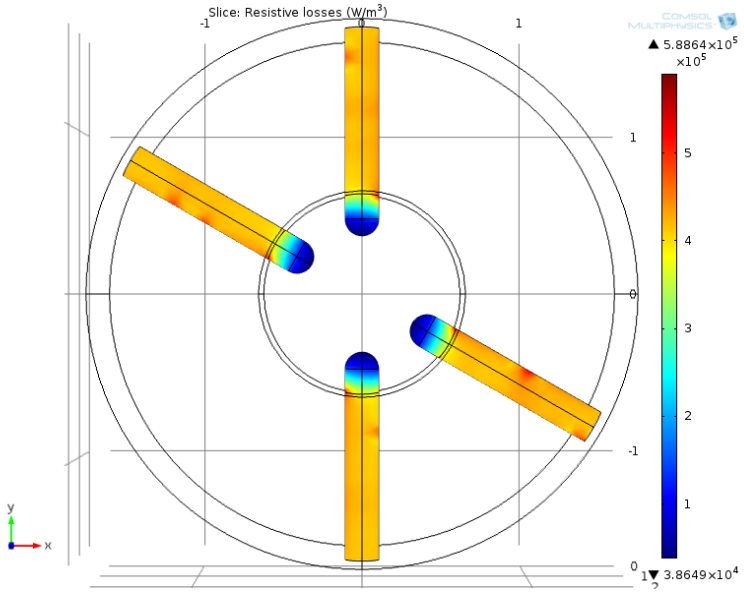

Figure 10: Joule effect (W/m^3) in the electrodes. Horizontal view

losses are symmetrically distributed with respect to the meridional plane of the electrodes.

The aforementioned images were obtained from the values of the geometrical parameters stated in Table 1. In Fig. 14 we have also represented the

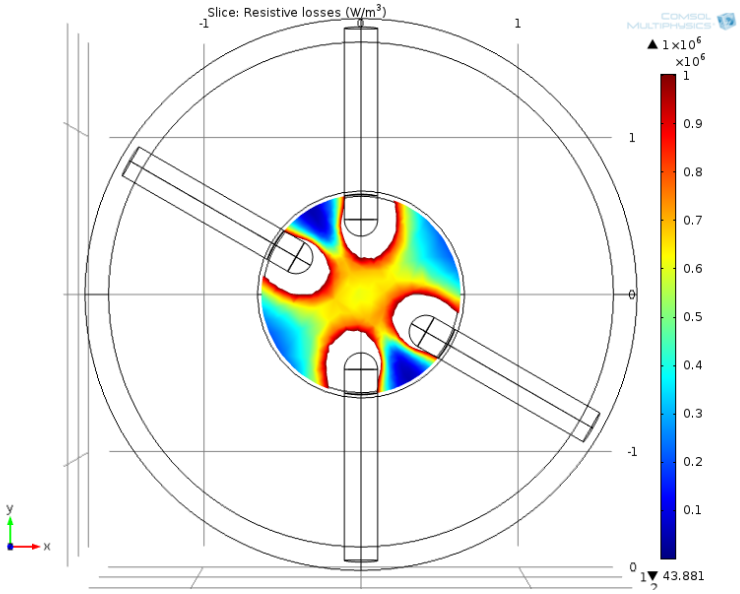

Figure 11: Joule effect (W/m^3) in the slag. Scale range. Horizontal view

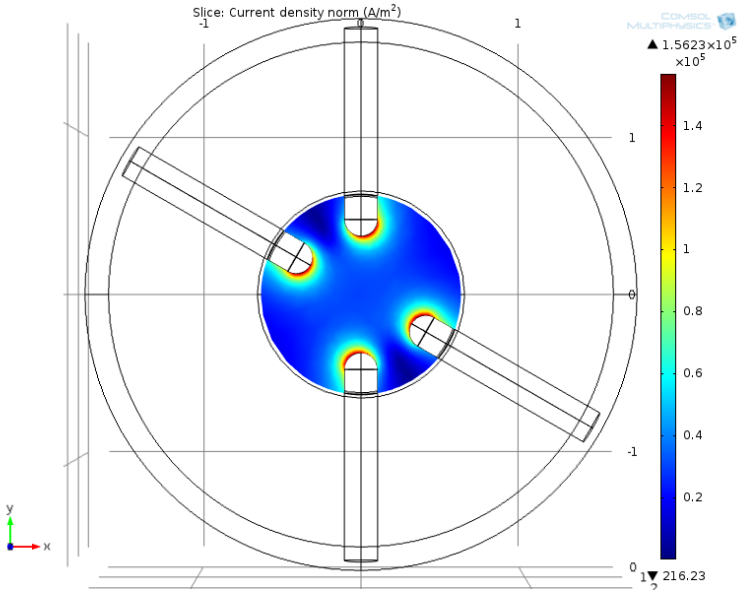

Figure 12: Current density norm (A/m^2) in the slag. Horizontal view

current density by assuming that the parameter h_t is smaller than that of Fig. 13. This new computation represents a situation where the amount of slag in the pot is less than in the previous case. As we can see, in this case more current flows from the electrodes to the metal. Again, for presentation

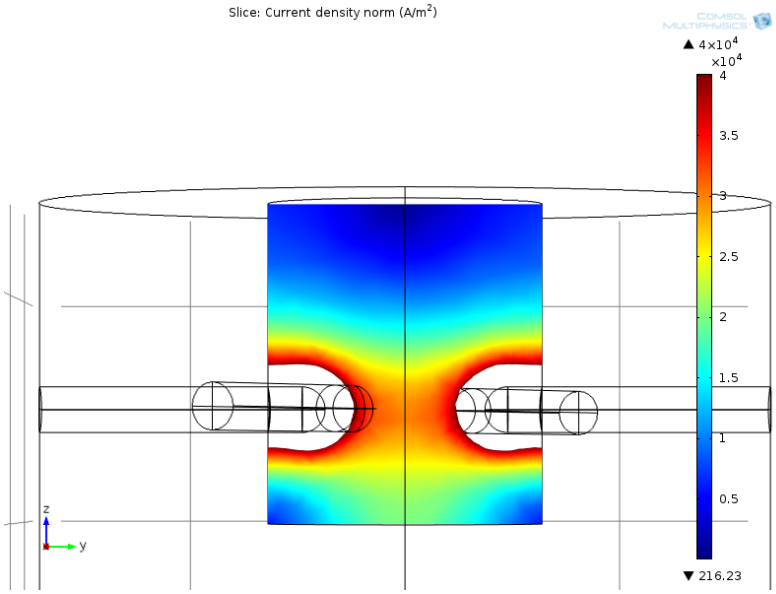

Figure 13: Current density norm (A/m^2) in the slag for h_t=1400 mm.

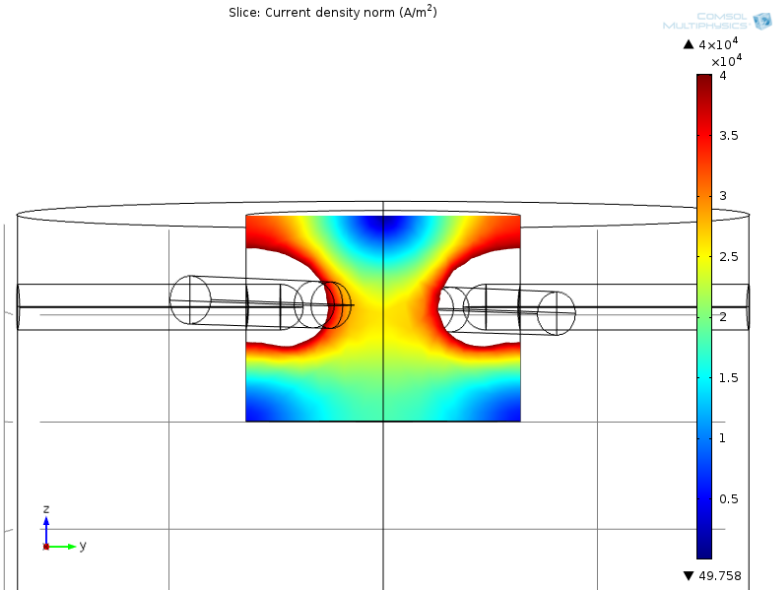

Figure 14: Current density norm (A/m^2) in the slag for h_t=900 mm.

purposes we have removed the maximum values of the field.

Due to the geometry parametrization, as highlighted, these kinds of changes in geometry are quite easy to make.

3.3.5 Numerical results for the three-electrode configuration

In this section we show some of the results obtained from the numerical simulation of the three-electrode system (see Fig. 15) when considering the geometrical and physical parameters summarized in Tables 2 and 3.

Since, we know the current intensity flowing through each electrode, we provide the RMS value of the alternating current and the phase in each electrode, with a counterclockwise advance of phase of 120°. Recall that, as mentioned in Section 3.3.2, the data used in Comsol Multiphysics® is the current density.

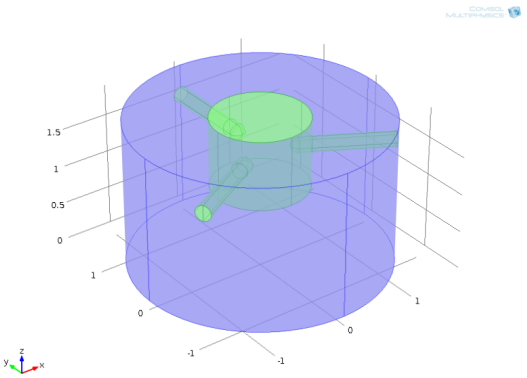

Figure 15: Domain with the three-electrode configuration.

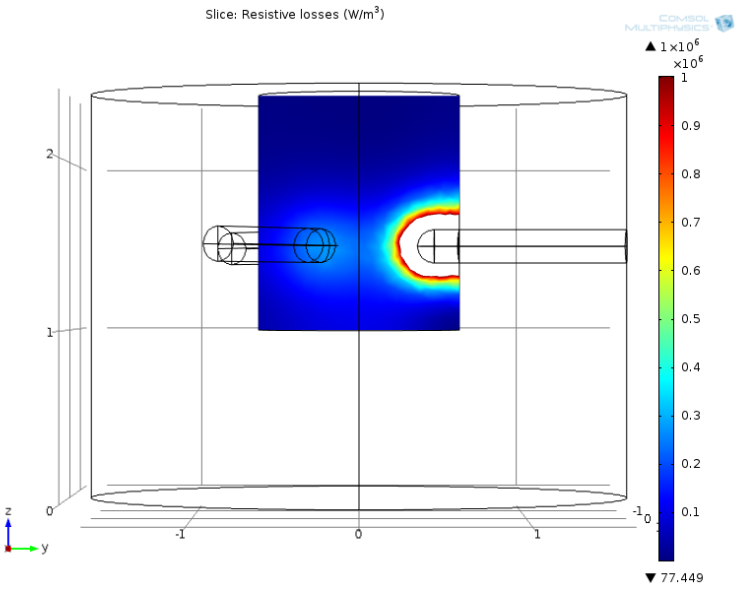

Figure 16: Joule effect (W/m^3) in the slag. Scale range

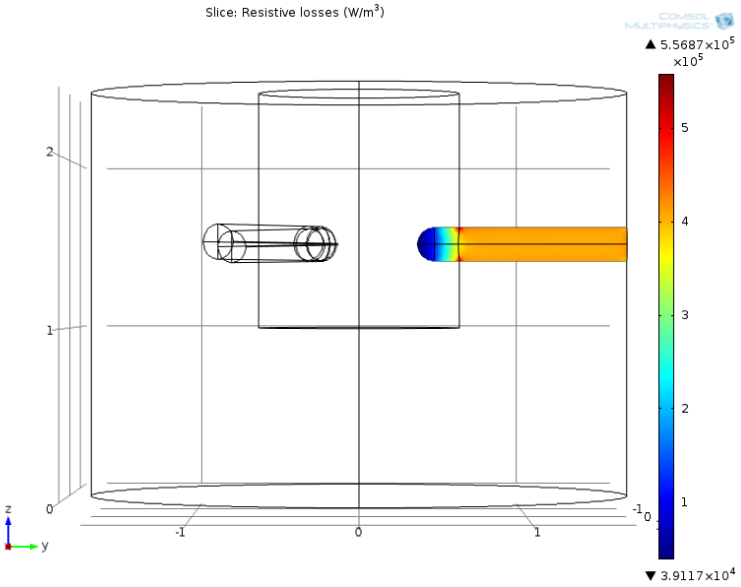

Figure 17: Joule effect (W/m^3) in the electrodes

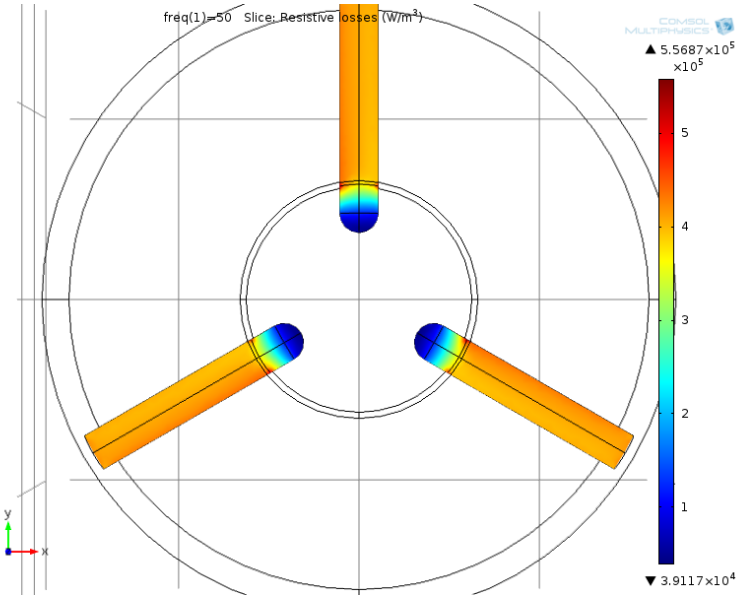

Figure 18: Joule effect (W/m^3) in the electrodes. Horizontal view

The Joule effect in the slag and in the electrodes is shown in Figures 16 and 17. In Fig. 16 we have removed the maximum values of the field for demonstration purposes. Figures 17 and 18 show the resistive losses in the electrodes from different plane views; Fig. 19 shows resistive losses in the slag.

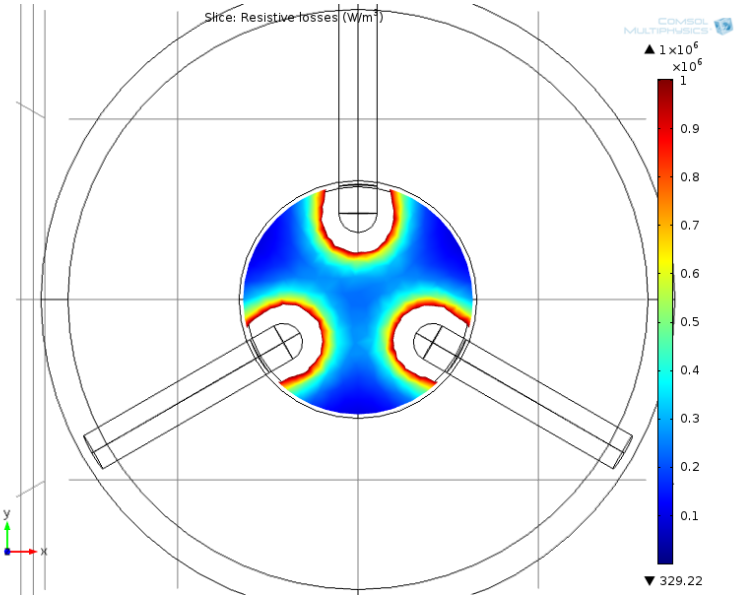

Figure 19: Joule effect (W/m^3) in slag. Scale range. Horizontal view

3.3.6 Some other results for the three-electrode system

In this section we show the resistive losses dissipated in the different parts of the three-electrode system while changing some of the geometrical parameters stated in Table 1. First, in Table 4 we consider different values for the parameters d_t and d_e, the diameter of the slag tank and the electrodes, respectively. We can deduce that, for a fixed value of d_e resistive losses in the slag and total losses increase with d_t. Analogously, for d_t fixed, the resistive losses in the slag and the total losses increase with d_e.

d_e (mm)	d_t=1200 (mm)	d_t=1400 (mm)	Region
200	3.83933E+04	3.85337E+04	electrodes
	3.10438E+05	3.28754E+05	slag
	1.02500E−02	1.10100E−02	air
	3.48831E+05	3.67288E+05	total
400	1.86131E+05	1.84224E+05	electrodes
	2.89721E+06	3.30162E+06	slag
	6.36200E−02	7.76100E−01	air
	3.08334E+06	3.48584E+06	total

Table 4: Resistive losses (W/m^3) in the three-phase system when changing d_e and d_t.

Region	h_t=1400 (mm)	h_t=2200 (mm)
electrodes	3.83933E+04	3.83974E+04
slag	3.10438E+05	3.11171E+05
air	1.02500E−02	1.07700E−02
total	3.48831E+05	3.49568E+05

Table 5: Resistive losses (W) in the 3 three-phase system when changing h_t.

Region	actual values (mm)	doubling values (mm)
electrodes	3.83933E+04	3.56964E+05
slag	3.10438E+05	2.86458E+06
air	1.02500E−02	1.04540E−01
total	3.48831E+05	3.22154E+06

Table 6: Resistive losses (W) in the three-phase system when doubling all geometrical parameters.

four electrode system	6.60223E+05
three electrode system	3.48831E+05

Table 7: Resistive losses (W) for the different configurations. Parameters values as in Table 1.

On the contrary, from Table 5, we deduce that as parameter h_t increases the resistive losses are practically the same.

In Table 6 we compare the losses when using the reference values stated in Table 1 with these values doubled. The losses are multiplied approximately by a factor of 10.

Table 7 summarizes the total resistive losses for both the four and three-electrode configurations, for geometrical and operation parameters detailed in Tables 1 and 2. These results show that, for the same parameter values, the three-phase system dissipates less power than the four-electrode one.

4. Thermal study for a single electrode

4.1. Mathematical model

In this section we consider the temperature evolution of one of the electrodes. Due to the physical description of the electrode we use a cylindrical coordinate system (r^*, θ^*, z^*) aligned with the cross section of the electrode, as shown in Fig. 1. We note that the * notation denotes dimensional variables. The length and radius of the electrode are denoted L and R, respectively. The electrode is aligned such that its axis coincides with the z-axis. The ends of the electrode are located at $z^* = 0$ and $z^* = L$.

The steady state temperature, T^*, in the electrode is modelled via the heat equation

$$\frac{1}{r^*}\frac{\partial}{\partial r^*}\left(k^*(T^*)r^*\frac{\partial T^*}{\partial r^*}\right)+\frac{1}{r^{*2}}\frac{\partial}{\partial \theta^*}\left(k^*(T^*)\frac{\partial T^*}{\partial \theta^*}\right)+\frac{\partial}{\partial z^*}\left(k^*(T^*)\frac{\partial T^*}{\partial z^*}\right)+Q=0\,, \tag{31}$$

where $k^*(T^*)$ is the temperature dependent thermal conductivity and Q is the Joule heating source term given by

$$Q = \frac{|J^2|}{2\sigma}\,, \tag{32}$$

where σ is the electrical conductivity and J is the amplitude current density [5]. Assuming a uniform temperature around the electrode, we neglect the θ^* dependence in the model, and hence, the θ^* partial derivative in (31) is ignored.

To complete the model, at the surface of the electrode we prescribe Newton's law of cooling boundary conditions of the form

$$-k^*(T^*)\frac{\partial T^*}{\partial n^*} = h(T^* - T_A)\,, \tag{33}$$

where h is the surface heat transfer coefficient and T_A is the ambient temperature of the surrounding medium. Inspection of Fig. 1 reveals that we require conditions at the ends of the electrode $z^* = 0$ and $z^* = L$. In addition, boundary conditions are needed at the curved surface of the electrode. These particular boundary conditions will depend on the surrounding medium, i.e., the slag or the outer casing of the reactor. Hence, there is a discontinuity in the boundary condition on the curved surface of the electrode. This suggests the use of a numerical method to solve for the temperature distribution of the electrode. We ignore this method here, and instead focus on a simple dimensional analysis.

4.2. Nondimensionalisation and dimensional analysis

The method of nondimensionalisation is applied to reduce the number of physical parameters, and simplify the model. We define the dimensionless variables

$$r^* = rR\,, \qquad z^* = zL\,, \qquad k^* = k_0 k\,, \qquad T^* = \Delta T T\,, \tag{34}$$

where k_0 is a reference thermal conductivity and the temperature scale ΔT is as yet unknown. Neglecting the θ dependence and substituting the dimensionless variables into (31) yields the dimensionless heat equation

$$\frac{1}{r}\frac{\partial}{\partial r}\left(k(T) r \frac{\partial T}{\partial r}\right) + \epsilon^2 \frac{\partial}{\partial z}\left(k(T)\frac{\partial T}{\partial z}\right) + \frac{|J^2|R^2}{2\sigma k_0 \Delta T} = 0\,, \tag{35}$$

where $\epsilon = R/L$ is the electrode aspect ratio. The radius and length of the electrode are 0.1m and 0.3m, respectively, and hence $|\epsilon^2 \ll 1$. Consequently, equation (35) can be simplified to

$$\frac{1}{r}\frac{\mathrm{d}}{\mathrm{d}r}\left(k(T) r \frac{\mathrm{d}T}{\mathrm{d}r}\right) + \frac{|J^2|R^2}{2\sigma k_0 \Delta T} + \mathcal{O}(\epsilon^2) = 0\,. \tag{36}$$

Assuming the thermal conductivity is temperature independent, (35) can be rewritten as

$$\frac{1}{r}\frac{\mathrm{d}}{\mathrm{d}r}\left(r \frac{\mathrm{d}T}{\mathrm{d}r}\right) + \frac{|J^2|R^2}{2\sigma k^* \Delta T} = 0\,, \tag{37}$$

where we have exploited $k^* = k k_0$. By assuming the electrical conductivity to be constant and large skin depth (30) compared to the electrode radius R, the current density J will not vary significantly over the cross-section of the electrode. Thus, the last term in (37) is approximately constant. The temperature variation is driven by the source term in (37) and so we choose the temperature scale to be

$$\Delta T = \frac{|J^2|R^2}{k^* 2\sigma}\,, \tag{38}$$

and hence (37) reduces to

$$\frac{1}{r}\frac{\mathrm{d}}{\mathrm{d}r}\left(r \frac{\mathrm{d}T}{\mathrm{d}r}\right) + 1 = 0\,. \tag{39}$$

The general solution to (39) is

$$T(r) = -\frac{r^2}{4} + C_0 \ln r + C_1\,, \tag{40}$$

where C_0 and C_1 are integration constants. Given the appropriate boundary conditions, (39) provides the temperature distribution in the electrode. The

unknown constants depend on whether the electrode surface is in thermal contact with the slag or the reactor casing.

Ignoring the precise details of (40) we return to the definition of the Joule effect heat source term. The current density for the cross section of the electrode is

$$J = \frac{\sqrt{2} I_{rms}}{A}, \tag{41}$$

where I_{rms} is the total rms current flowing through the electrode and $A = \pi R^2$ is the cross-sectional area of the electrode. Hence, the temperature scale given by (38) can be rewritten as

$$\Delta T = \frac{I_{rms}^2}{\pi^2 R^2 k^* \sigma}. \tag{42}$$

The above expression shows that for a fixed ΔT, the current I is proportional to the radius of the electrode.

5. Conclusions

The study group working in this problem focused on examining two different aspects: on one hand, the mathematical modelling and numerical simulation of the electromagnetic process; on the other, the statement of a nondimensional model dealing with the thermal phenomena.

Concerning the electromagnetic problem, a mathematical model has been proposed and some numerical computations performed. A parameterized code that can be used to compute the solution for different geometrical and physical parameters has been built using the Comsol Multiphysics® software. The preliminary computations show that the same dimensions of the furnace and same intensity, the three-phase system dissipates less power than a one-phase configuration.

We considered a thermal model for the temperature evolution of a single electrode. The dimensional analysis indicates a proportional relationship between the electrode radius and the current. A discontinuity in the surface temperature requires the use of an appropriate numerical simulation. In the future the thermal model should be coupled with the electromagnetic problem to obtain a complete description of the process.

The process taking place within the reactor is truly multi-physics, with couplings between heat transfer, chemical reactions and electrical phenomena. For a real study of the process a mathematical model including all these aspects should be considered. In this sense, the thermal dimensionless model proposed on the second part of this document is a first step in this direction.

References

[1] A. Alonso Rodríguez and A. Valli, *Eddy current approximation of Maxwell equations, ser. MS&A. Modeling, Simulation and Applications*, Springer-Verlag, Milan, Italia, vol. 4, 2010.

[2] A. Bermúdez, D. Gómez, P. Salgado, *Mathematical models and numerical simulation in electromagnetism*, Springer-Verlag, Milan, Italia, vol. 74, 2014.

[3] A. Bermúdez, R. Rodríguez, and P. Salgado, FEM for 3D eddy current problems in bounded domains subject to realistic boundary conditions. An application to metallurgical electrodes, *Computer Methods in Applied Mechanics and Engineering*, **12**, (2005) no. 1, pp. 67–114.

[4] A. Bossavit, *Computational electromagnetism*, Academic Press Inc., San Diego, CA, 1998.

[5] H. Fangohr, D.S. Chernyshenko, M. Franchin, T. Fischbacher, and G. Meier, Joule heating in nanowires, *Physical Review B* **84** (2011), no. 5, 054437.

[6] V. Girault,P.A. Raviart, *The finite element method for Navier-Stokes equations*, Springer-Verlag, New York, 1986.

Electric Scale-up for a slag heating furnace

Academic coordinator Alfredo Bermúdez, Dolores Gómez
Institution Universidade de Santiago de Compostela (USC) and Instituto Tecnológico de Matemática Industrial (ITMATI)

Specialist Rafael Vázquez
Institution Istituto di Matematica Applicata e Tecnologie Informatiche

Business coordinator Svenn Anton Halvorsen
Company Teknova AS

Team Vincent Cregan (Centre de Recerca Matemática. Universitat Autónoma de Barcelona), Francisco Pena (Universidade de Santiago de Compostela and Instituto Tecnológico de Matemática Industrial), Ángel Rial (Universidade de Santiago de Compostela), Rune Schlanbusch (Teknova AS)